

# ACCELERATING STRUCTURE FOR C-BAND ELECTRON LINEAR ACCELERATOR OPTIMIZATION

S.V. Kutsaev, N.P. Sobenin, A.A. Anisimov, Moscow Engineering-Physics Institute (State University), Moscow, Russian Federation  
 M. Ferderer, A.A. Zavadtsev, A.A. Krasnov, Identification Beam Systems LLC, Atlanta, USA

## Abstract

This paper presents the results of a survey study that analyzed and compared several linear accelerator designs operating in the range of 5 to 20 MeV for use in advanced cargo inspection systems. These designs were based on klystron generated RF power input of 3.2 and 4.5 MW at 5712 MHz. Several different accelerating structures were considered including standing wave (SW) and travelling wave (TW) structures. In addition several hybrid structures, composed of a SW buncher sections and TW accelerator sections, were included in the study. Cells geometries and beam dynamics parameters, for these accelerating structures, were calculated using advanced numerical simulation methods. Accelerating structures and input couplers for SW and hybrid structures were designed.

## INTRODUCTION

Cargo inspection systems should be simple, compact and highly reliable. Historically S-band liner accelerators have been used for this application. By using a higher frequency structure we can significantly increase the shunt impedance and therefore provide necessary energy gain with a shorter structure length. The effective shunt impedance of a 5712 MHz biperiodic structure is 30% greater than a 2856 MHz structure while the external diameter is approximately half the diameter. In addition to the cavity being significantly smaller waveguides and other RF components are as well. To facilitate large capture coefficients, without using an external focusing magnet, SW biperiodic structure bunchers were used. Along with the SW biperiodic structures, hybrid structures are of particular interest for this type of application.

Modern cargo systems need to generate more than a black and white image to be effective in solving the cargo security problem that the world is facing. To be effective the systems must also generate material based information. In particular, Z-function and density information needs to be presented to the operators. To obtain Z-function and density information the accelerator must be able to vary output energy from pulse to pulse.

## SW STRUCTURE

In designing SW biperiodic accelerating structures it is important to ensure that the necessary beam parameters are met without requiring unrealistic manufacturing tolerances. To satisfy this requirement the coupling coefficient ( $k_c$ ) was increased to 11 percent from the more traditional range of 4 to 5 percent.

Cell tuning to the required frequency and field distribution was performed using the resonant models. In Figure 1 a resonant model for the regular cell and the distribution of longitudinal component of electric field on axis are illustrated.

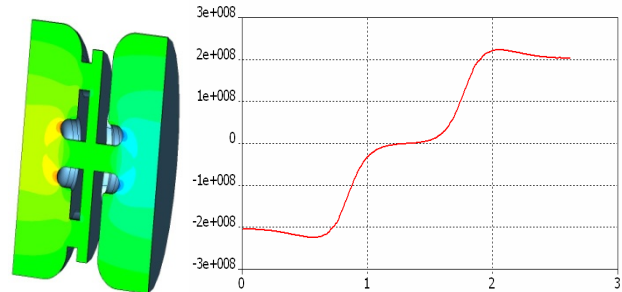


Figure 1: Resonant model of the regular cell and the distribution of electric field in it.

For constructional convenience the RF power is input into the first cell. Two WR187 waveguides are connected to the first cell symmetrically to provide symmetry of the field in this cell. One of these waveguides is short-circuited by the metal pin and is used for vacuum pumping. Figure 2 shows the model of this coupler as well as electric field intensity.

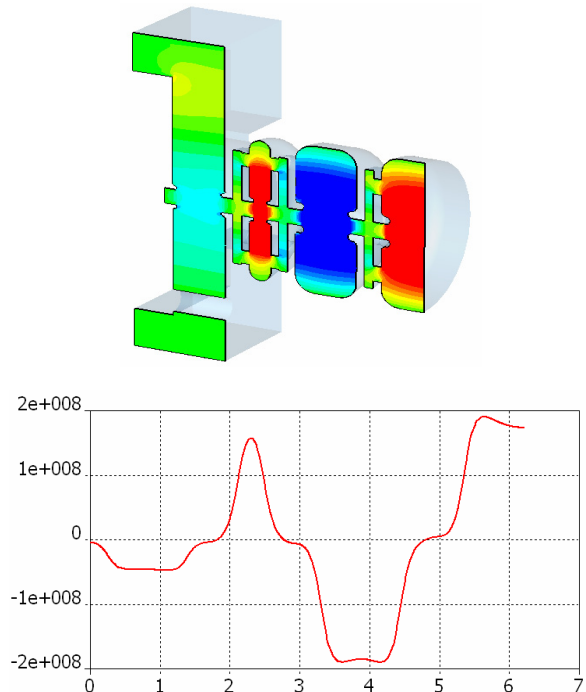


Figure 2: Distribution of electric field in SW buncher.

Table 1: SW Structure Parameters

Cell number	Phase velocity	Effective shunt impedance, MOhm/m	Coupling coefficient, %	Q-factor
1	0.67	50.3	38.9	5540
2	0.42	28.2	13.5	5680
3	0.78	97.6	10.9	6800
4, 5...	0.99	114.2	11.0	9770

The calculations for two C-band structures, with a different number of accelerating cells, were performed. In addition, energy variation capability was evaluated for these two structures. The first accelerator had output energies in the range of 3-7 MeV while the second one had output energies in the range of 11-15 MeV. Energy variation capability was evaluated by adjusting the injected current. The results of beam dynamics calculations for these accelerators are presented in Table 2 ( $W_{av}$  is average energy of accelerated electrons,  $I_{out}$  is output beam current,  $I_{in}$  is injected beam current,  $k_c$  is capture coefficient,  $L$  is structure length,  $P_b$  is beam power,  $P_{in}$  is input RF power.). The dependency of output energy as function of input current for these two accelerator structures is illustrated in Figure 3.

Table 2: Results of Particle Dynamics Calculations

$L$ , m	$k_c$ , %	$P_{in}$ , MW	$W_{av}$ , MeV	$I_{out}$ , mA	$k_c$ , %	$P_b$ , MW
0.97	57.2	4.5	15	86	57.2	1.43
0.97	51.5	4.5	11	195	51.5	2.48
0.44	50.6	3.3	7	230	50.6	1.82
0.44	38.6	3.3	3	730	38.6	2.92

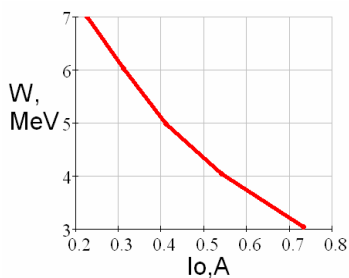
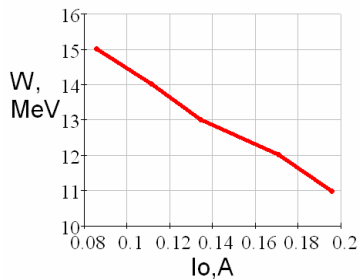


Figure 3: Output energy of 11-15 MeV structure (left) and 3-7 MeV structure (right) as functions of current.

### HYBRID STRUCTURE

Along with SW structure presented above several hybrid structures were considered. The analyzed hybrid structures consisted of a SW-buncher section combined with TW accelerating sections. Accelerating cells in the TW sections can be coupled by electric field through on-axis wholes (disk-loaded structure – DLS) [1-3] or by magnetic field through periphery slots (Figure 4) with negative (NDS) or positive (PDS) dispersion [4].

Calculated PDS electro-dynamic characteristics depending on operating mode  $\Theta$  are shown in Table 3 ( $a$  is aperture diameter,  $\lambda$  is wave length,  $R_{sh}$  is shunt impedance,  $\alpha$  is attenuation factor,  $\beta_{gr}$  is relative group velocity,  $\tau = \alpha L$ ).

Table 3: Parameters of PDS Hybrid Structure

$\Theta$	$a/\lambda$	$R_{sh}$ , MOhm/m	Q	$\alpha$ , 1/m	$\beta_{gr}$ , %	$\tau$
$3\pi/2$	0.1	95	11130	0.059	9.1	0.11
$4\pi/3$	0.1	123	10310	0.096	6.3	0.12
$5\pi/4$	0.1	92	9420	0.146	4.4	0.18
$6\pi/5$	0.1	96	9072	0.171	3.9	0.19

Main electro-dynamic characteristics of DAL, PDS and NDS as a functions of  $a/\lambda$  at relative phase velocity 0.999 are presented in Table 4. It can be seen that shunt impedance of the structures decreases as the aperture diameter is increased.  $\tau$  corresponds to TW section for  $W_{av}=10$  MeV,  $P_{in}=4.1$  MW,  $I_{out}=0.1$  A.

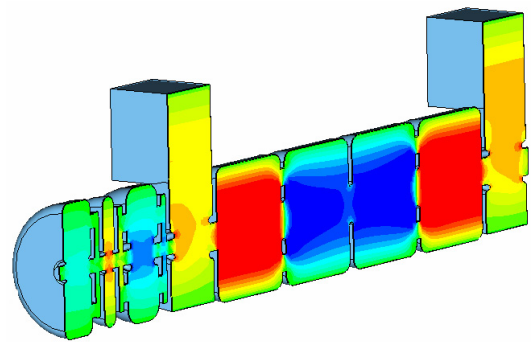


Figure 4: Magnetic coupled TW structure with SW Buncher.

Common input coupler is used for SW buncher and for TW accelerating structure.

If TW accelerating structure is based on DLS or PDS, input coupler is coupled with last cell of the buncher and with first cell of the TW accelerating structure. Input waveguide is located between the buncher and the TW accelerating structure.

If TW accelerating structure is based on NDS, input coupler is coupled with last cell of the TW accelerating structure. RF power, passing through the whole TW accelerating structure, comes into the buncher through coupling whole between first cell of the TW accelerating structure and last cell of the buncher.

Table 4: Parameters of Different TW Sections

$a/\lambda$	Type	$\Theta$	$R_{sh}$ , MOhm /m	Q- factor	$\alpha$ , 1/m	$\beta_{gr}$ , %	$\tau$
0.04	PDS	$5\pi/4$	122	9750	0.121	4.5	0.11
	NDS	$3\pi/4$	86	7400	0.145	5.9	0.18
0.07	PDS	$5\pi/4$	111	9950	0.126	4.5	0.12
	NDS	$3\pi/4$	73	7520	0.151	5.5	0.16
0.10	PDS	$5\pi/4$	92	9420	0.146	4.5	0.14
	NDS	$3\pi/4$	56	7130	0.156	5.7	0.19
	DLS	$2\pi/3$	87	9070	0.660	1.0	0.35
0.12	PDS	$5\pi/4$	84	9430	0.150	4.4	0.15
	NDS	$3\pi/4$	49	7300	0.148	5.7	0.20
	DLS	$2\pi/3$	65	9000	0.330	1.9	0.27
0.14	PDS	$5\pi/4$	69	8700	0.156	4.4	0.17
	NDS	$3\pi/4$	39	6700	0.173	5.4	0.25
	DLS	$2\pi/3$	65	9000	0.200	3.2	0.20

Using the parameters from Tables 3 and 4, the beam dynamics calculations were done for two structure types: DLS and PDS. In both accelerators the buncher is the same to the one used for the SW accelerator. All calculations were done for 10 MeV energy and 100 mA beam current. The accelerating sections are considered to be with constant impedance. The results of these calculations are presented in Table 5.

Table 5: Results of Particle Dynamics Calculations

Structure	$W_{av}$ , MeV	$I_{out}$ , mA	$k_c$ , %	$L$ , m	$P_{in}$ , MW
DLS	10	99	65.8	0.8	4.5
PDS	10	96	63.8	1.1	4.5

### CONSTRUCTION

3D engineering design of SW accelerating structure is shown in Figure 5.

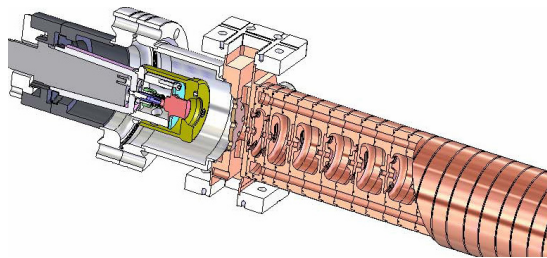


Figure 5: SW accelerating structure with the injector.

3D engineering design of irradiator of the accelerator is shown in Figure 6.

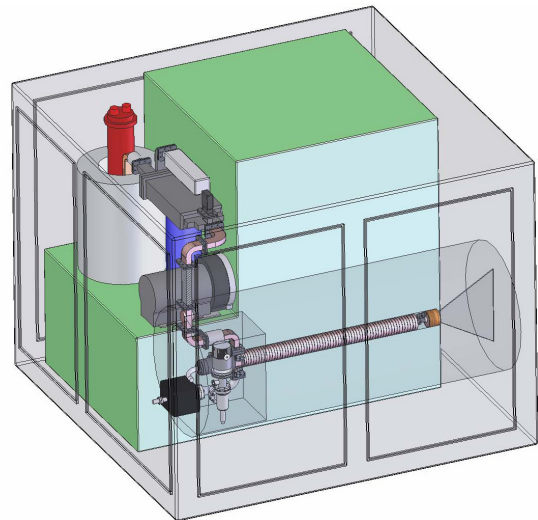


Figure 6: Irradiator.

The irradiator includes SW accelerating structure, injector, W-target, klystron, circulator, directional coupler, waveguide window, vacuum system, modulator and lead local shielding (shown transparent). Overall dimensions of the irradiator are 1.8x1.8x1.4 m.

### CONCLUSIONS

Several linear electron beam accelerator structures for cargo inspection applications have proposed. Electrodynamic characteristics for a pure SW structure and different types of Hybrid (SW buncher plus TW accelerating section) structures were calculated. Variable energy control was studied for the SW structure. Particle dynamics for the SW structure and Hybrid structures (PDS and DLS) was calculated. A common input coupler and bunching sections was designed for the SW and Hybrid structures. The use of compact C-band accelerating structure allows us to build very compact and effective irradiator for cargo inspection system.

### REFERENCES

- [1] O.A.Valdner, N.P.Sobenin, B.V.Zverev, I.S. Shedrin, "Disk-Loaded Waveguides", 3<sup>rd</sup> Edition, 1991, Energoatomizdat.
- [2] N.P.Sobenin, B.V.Zverev, "Electrodynamical characteristics of accelerating cavities", 1999, Foundation of International Scientific and Educational Cooperation, London, England.
- [3] Yu.V.Zuev, M.A.Kalinichenko, A.V.Ryabtsov, I.V.Chetverikov, "Accelerating structure of electron linear accelerator UELV-10/5-15C", Preprint CNIAtomInform, 2001.
- [4] D.Tronc, "Linac accelerating structures", Proceeding EPAC'94.